Inorganica Chimica Acta 406 (2013) 307–314

Contents lists available at SciVerse ScienceDirect

Inorganica Chimica Acta

journal homepage: www.elsevier.com/locate/ica

Distinct structures of inorganic–organic supramolecular assemblies based on discrete metallocyclic complexes incorporating flexible imidazole ligands: Syntheses, crystal structures and properties

Li Yang [a,*], Guanjun Chang [a], Liang Luo [b], Feng Ding [a], Jingsong You [b]

[a] State Key Laboratory Cultivation Base for Nonmetal Composites and Functional Materials, School of Materials Science and Engineering, Southwest University of Science and Technology, 59 Qinglong Road, Mianyang 621010, PR China
[b] Key Laboratory of Green Chemistry and Technology of Ministry of Education, College of Chemistry, Sichuan University, 29 Wangjiang Road, Chengdu 610064, PR China

ARTICLE INFO

Article history:
Received 23 April 2013
Received in revised form 6 July 2013
Accepted 10 July 2013
Available online 19 July 2013

Keywords:
Discrete metallocyclic structure
Flexible
Imidazole ligand
Supramolecular building blocks
Secondary interaction

ABSTRACT

Three new interesting discrete dinuclear metallocyclic complexes, namely, $\{[Pd_2(\mathbf{1})_4](NO_3)_4{\cdot}2DMSO{\cdot}2H_2O\}_n$ (**4**), $[Pd_2(\mathbf{2})_2Br_4]_n$ (**5**), and $\{[Pd_2(\mathbf{3})_2Cl_4]{\cdot}4DMSO\}_n$ (**6**) have been successfully synthesized by the reaction of flexible exo-bidentate imidazole-containing ligands 1,3-bis(imidazol-1-ylmethyl)benzene (**1**), 1,3-bis(imidazol-1-ylmethyl)-5-methylbenzene (**2**), and 2,6-bis(imidazol-1-ylmethyl)-4-*tert*-butylphenol (**3**) with corresponding palladium salts. All these complexes were characterized by NMR spectroscopy in combination with elemental analysis, powder X-ray diffraction (PXRD), single-crystal X-ray diffraction, and thermal gravimetric analysis (TGA), respectively. Though all three complexes involve the similar supramolecular building blocks [2+2] metallocyclic units, under the inducement effect of the organic ligands, compounds **4**–**6** exhibit delicate geometric diversification of the resulting high-dimensional inorganic–organic supramolecular assemblies (e.g., [4+2] lantern-like cage structure, 1D channel, and 2D undulating framework, respectively). Furthermore, these results demonstrate that the secondary interactions such as intermolecular $\pi\cdots\pi$ stacking interactions and hydrogen bonds could play important roles in the aspect of linking low-dimensional entities into high-dimensional supramolecular frameworks.

1. Introduction

In recent decades, the designed construction of new crystalline materials with intriguing aesthetic structures and topological features has been a highly active area of investigation [1], due to their unique potential applicability as functional materials in many areas such as gas sorption [2], photochemistry [3], molecular magnetism [4], nonlinear optics [5], heterogeneous catalysis [6], and ion-exchange [7]. However, it is still a great challenge to rational design and controllable synthesis of the desired crystalline solids through the construction of coordination bonding and other supramolecular contacts to interconnect various molecular building tectons. It is well known that the complexity of the factors [8], such as coordination requirement of the central metal ions, the nature of ligands, metal–ligand ratio, solvent, temperature, and counterions etc., have significant influences on the resulting frameworks, rendering it difficult to predict the molecular architectures under certain circumstances. Literature survey shows that one of the key issues for the preparation of the coordination compounds with novel structures is the proper design and careful selection of organic ligands with suitable binding groups [9]. In this field, organic ligands act as bridging links between metal fragments, which are of utmost importance because of the different spacer lengths, flexibility, steric hindrance effects, and conformational preferences in the self-assembly process [10]. Therefore, considerable attentions have been devoted to the prospect of controlling the properties and structures of metal–organic supramolecular assemblies by selection of proper organic ligands [11]. Among the examples reported, linear, rigid, and bifunctional bridging ligands with an adjustable arene core have been found to be one of the most versatile building blocks.

The self-assembly through metal–ligand-directed interaction to provide discrete molecular metallacyclic rings or cages capable of encapsulating guest moieties has garnered attention lately. Mirkin [12,13] and Stang et al. [14,15] have developed the various design methodologies behind coordination-driven self-assembly by using flexible ligands to afford a variety of discrete metallacycles and metallacages with well-defined shapes and sizes. Such materials have great application potential for separation processes, recognition, catalysis, bioimaging, and sensor technologies. Therefore, exploration into discrete macrocyclic coordination complexes

* Corresponding author. Tel./fax: +86 816 2419201.
E-mail address: liyang@swust.edu.cn (L. Yang).

0020-1693/$ - see front matter © 2013 Elsevier B.V. All rights reserved.
http://dx.doi.org/10.1016/j.ica.2013.07.014

through harmonizing the subtle relationship between "robustness" and "flexibility" in these systems has attracted much recent interest. As we know, flexible imidazole ligands with $(-CH_2-)_n$ (n = 1, 2, 3) spacers as a critically important family of building blocks are reliable candidates for assembly of diverse supramolecular complexes with fascinating topologies (e.g., one-dimensional (1D) chain or channel, two-dimensional (2D) network and three-dimensional (3D) architecture) and peculiar physicochemical properties owing to the excellent coordination ability of the imidazole ring [16]. On the other hand, the flexible nature of the alkyl $(-CH_2-)_n$ spacer allows the ligands to bend and rotate freely so as to be used as "organic clips" to bind transition metal ions into neutral bimetallic macrorings or cages [16d,17].

Recently, we have designed and synthesized a series of bent restricted bidentate pyrazole bridging spacers coordinated with silver salts for construction of dinuclear metallocyclic complexes [18]. As part of our ongoing interests in the *N*-heterocyclic chemistry [19,20], we have also used the flexible bismethylimidazolyl derivatives self-assembling with $Pd(OAc)_2$ to generate a switching of metal–organic vesicles to globular networks depending on whether the ligands bear the hydroxyl groups [21]. Considering the bent geometry of such spacers, we wondered if these ligands could bind metal ions to give new self-assembly architectures and topologies such as dinuclear metallocycles. In this study, we select the flexible exo-bidentate imidazole-containing ligands **1**–**3** (Scheme 1) and different divalent palladium salts to synthesize three new metal–organic assemblies, namely, $\{[Pd_2(\mathbf{1})_4](NO_3)_4\cdot 2DMSO\cdot 2H_2O\}_n$ (**4**), $[Pd_2(\mathbf{2})_2Br_4]_n$ (**5**), and $\{[Pd_2(\mathbf{3})_2Cl_4]\cdot 4DMSO\}_n$ (**6**). The new compounds have been characterized by ^{1}H NMR spectroscopy, elemental analysis and X-ray crystallography. The results show that all of these supramolecular complexes are composed of the discrete dinuclear metallocyclic units. Besides the highly essential metal–ligand interactions that are basically responsible for coordination assemblies, there exist a variety of other secondary interactions such as π···π stacking interactions, hydrogen bonds (e.g., O–H···O, C–H···O, C–H···Br), which also play significant roles in the aspect of extended arrays of these metallocyclic building motifs into high-dimensional supramolecular frameworks. More interestingly, the structural versatility of resulting aggregates strongly depends on the presence of additional functional sites in the aryl ring of chosen ligands.

2. Experimental

2.1. General remarks

^{1}H NMR spectra were obtained with a Bruker AV-400 (400 MHz) spectrometer, while ^{13}C NMR spectra were recorded with a Bruker AV-400 (100 MHz) spectrometer. Mass spectra were obtained on a Finnigan-LCQ^{DECA} instrument. Elemental analyses were performed with a CARLO ERBA1106 instrument. Melting points were determined with XRC-1 and are uncorrected. Thermal analyses were performed on a TA Q500 from room temperature to 750 °C with a heating rate of 10 °C min^{-1} under a N_2 atmosphere. Powder X-ray diffraction (PXRD) patterns were collected on a Philips X'PERT Pro MPDX powder diffractometer with Cu Kα radiation (1.54056 Å). The simulated PXRD spectra from single-crystal structures were carried out using Mercury (version 1.4.2, 2002) and were compared to confirm the composition of the crystal with the experimental PXRD pattern.

Unless otherwise noted, all reagents were obtained from commercial suppliers and used without further purification. Tetrahydrofuran (THF) was dried by heating at reflux for at least 8 h over sodium/benzophenone and freshly distilled prior to use. Ligands **1**, **2**, and **3** were synthesized according to our previously reported method [21].

2.2. Characterization of ligands **1**–**3**

2.2.1. 1,3-Bis(imidazol-1-ylmethyl)benzene (**1**)

Pale yellow solid. Yield: 56.3%. M.p. 53–55 °C. ^{1}H NMR (400 MHz, $CDCl_3$): δ 5.07 (s, 4H), 6.85 (dd, J = 1.2 Hz, 1.2 Hz, 2H), 6.90 (s, 1H), 7.06–7.09 (m, 4H), 7.30 (t, J = 5.9 Hz, 1H), 7.50 (s, 2H) ppm. ^{13}C NMR (100 MHz, $CDCl_3$): δ 50.4, 119.3, 125.9, 127.1, 129.7, 129.8, 137.2, 137.4 ppm. MS (ESI) m/z: 239 $[M+H]^+$.

2.2.2. 1,3-Bis(imidazol-1-ylmethyl)-5-methylbenzene (**2**)

Pale white solid. Yield: 67.9%. M.p. 105–106 °C. ^{1}H NMR (400 MHz, $CDCl_3$): δ 2.27 (s, 3H), 5.02 (s, 4H), 6.71 (s, 1H), 6.85 (dd, J = 1.2 Hz, 1.6 Hz, 2H), 6.86–6.87 (m, 2H), 7.05 (dd, J = 1.2 Hz, 1.2 Hz, 2H), 7.50 (s, 2H) ppm. ^{13}C NMR (100 MHz, $CDCl_3$): δ 21.2, 50.4, 119.3, 123.2, 127.8, 129.7, 137.1, 137.3, 139.8 ppm. MS (ESI) m/z: 253 $[M + H]^+$.

2.2.3. 2,6-Bis(imidazol-1-ylmethyl)-4-tert-butylphenol (**3**)

Pale yellow solid. Yield: 42.7%. M.p. 158–160 °C. ^{1}H NMR (400 MHz, DMSO-d_6): δ 1.15 (s, 9H), 5.17 (s, 4H), 6.87 (s, 2H), 7.02 (s, 2H), 7.14 (s, 2H), 7.69 (s, 2H), 9.23 (s, 1H) ppm. ^{13}C NMR (100 MHz, DMSO-d_6): δ 31.6, 34.2, 45.9, 120.1, 125.6, 126.6, 128.7, 137.9, 142.9, 150.5 ppm. MS (ESI) m/z: 310 $[M]^+$.

2.3. Synthesis of $\{[Pd_2(\mathbf{1})_4](NO_3)_4\cdot 2DMSO\cdot 2H_2O\}_n$ (**4**)

A DMSO solution (2 mL) of $Pd(NO_3)_2\cdot 2H_2O$ (26.6 mg, 0.1 mmol) was added slowly with constant stirring to a DMSO solution (2 mL) of **1** (23.8 mg, 0.1 mmol) to give an orange solution. The reaction mixture was stirred for 30 min and was then filtered to remove a trace amount of undissolved substance. Light yellow block crystals suitable for X-ray analysis were obtained by slow diffusion of acetone into the corresponding DMSO solution at ambient temperature after several days. Yield: 48%. *Anal.* Calc. for $C_{60}H_{72}N_{20}O_{16}Pd_2S_2$ (**4**): C, 44.86; H, 4.52; N, 17.44. Found: C, 44.50; H, 4.37; N, 18.07%.

2.4. Synthesis of $[Pd_2(\mathbf{2})_2Br_4]_n$ (**5**)

The title compound was prepared by the same procedure as compound **4** using **2** (25.2 mg, 0.1 mmol) instead of **1** and $PdBr_2(CH_3CN)_2$ (34.8 mg, 0.1 mmol) instead of $Pd(NO_3)_2\cdot 2H_2O$. Orange block crystals were obtained. Yield: 75%. *Anal.* Calc. for $C_{30}H_{32}N_8Pd_2Br_4$ (**5**)·2DMSO: C, 34.22; H, 3.72; N, 9.39. Found: C, 33.46; H, 3.68; N, 9.27%.

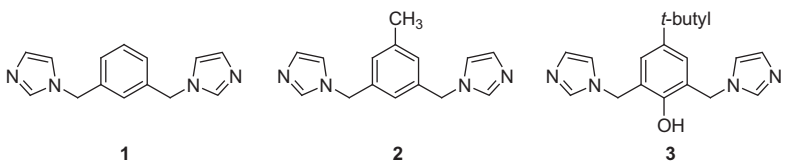

Scheme 1. Chemical structures of ligands **1**–**3**.

2.5. Synthesis of {[Pd_2(**3**)$_2Cl_4$]·4DMSO}$_n$ (**6**)

The title compound was prepared by the same procedure as compound **4** using **3** (31.0 mg, 0.1 mmol) instead of **1** and $PdCl_2(CH_3CN)_2$ (25.9 mg, 0.1 mmol) instead of $Pd(NO_3)_2·2H_2O$. Orange block crystals were obtained. Yield: 67%. *Anal.* Calc. for $C_{44}H_{68}Cl_4N_8O_6Pd_2S_4$ (**6**): C, 41.03; H, 5.32; N, 8.70. Found: C, 41.00; H, 5.28; N, 8.62%.

2.6. X-ray diffraction determination and refinement

X-ray single-crystal diffraction data for **4**, **5** and **6** were collected on a Bruker SMART 1000 CCD diffractometer at 100 or 120 K with graphite monochromated Mo Kα radiation (λ = 0.71073 Å) with ω scan mode. All the structures were solved by direct methods using the SHELXS program and refined by full-matrix least-squares methods with SHELXL [22]. Metal atoms in each complex were located from the *E*-maps and other non-hydrogen atoms were located in successive difference Fourier syntheses and refined with anisotropic thermal parameters on F^2. Hydrogen atoms were included in calculated positions and refined with constrained thermal parameters riding on their parent atoms. The non-coordinated solvent molecules of **5** could not be located in the difference map because of disorder. The crystal parameters, data collection and refinement results for the three compounds are summarized in Table 1. Selected bond lengths and angles are listed in Table 2. Full details of the crystallographic analyses are given in Supplementary material as CIF files.

3. Results and discussion

Complexes **4**–**6** were conveniently prepared at room temperature by diffusion methods with good yields. Slow diffusion of acetone into the corresponding DMSO solution of the ligand and corresponding palladium salt in a 1:1 M ratio yielded single crystals suitable for X-ray diffraction analysis. Elemental analyses of these complexes are consistent with the expected formulation of their structures. In addition, all of the obtained crystals (**4**–**6**) are instable in the presence of air, and are unsolvable in common solvents.

3.1. Formation of discrete dinuclear [Pd_2L_2] complexes

In this work, the solution behaviors of ligands **1**–**3** with corresponding divalent Pd^{2+} ions were initially investigated. The ^{1}H NMR studies indicate that the signals for the metal-free ligands disappear completely upon addition of an equimolar amount of metal ions and the quantitative formation of a single self-assembled architecture (see the Supporting Information). Due to metal coordination interactions between Pd(II) and the nitrogen atoms of the imidazole rings, the imidazole C2–H peaks undergo upfield shifts. Moreover, the H4 and H5 protons of the imidazole units, as well as the benzyl protons, also give rise to obvious upfield shifts (Fig. 1 and Figs. S1 and S2). As an example, the ^{1}H NMR spectrum of the mixture of **2** and $PdBr_2(CH_3CN)_2$ in a 1:1 ratio shows one set of new signals in a simple, highly symmetrical pattern, and the signals of ligand **2** disappear completely (Fig. 1). These results strongly suggest that the discrete, highly symmetrical dinuclear [Pd_2L_2] complexes can be exclusively formed by mixing ligands **1**–**3** and Pd(II) ions in solution.

3.2. Structural description of {[Pd_2(**1**)$_4$](NO$_3$)$_4$·2DMSO·2H_2O}$_n$ (**4**)

Single-crystal X-ray structural analysis reveals that **4** crystallized in monoclinic space group *C*2/*c*. The asymmetric unit consists of one Pd(II) ion, two flexible exo-bidentate ligands, two NO_3^- anions, one DMSO solvent molecule and one water solvent molecule. Notably, in the compound, two ligands connect two Pd(II) ions to achieve a distorted 38-membered [Pd_2(**1**)$_2$] dinuclear metallocyclic unit and further the two different metallocyclic rings doubly bridge to one another by means of the same metal atoms, resulting in the formation of an interesting [4+2] lantern-like cage structure (Fig. 2a). As illustrated in Fig. 2a, each Pd(II) centre is 4-coordinated by four N atoms (Pd–N(1)$^{\#1}$ = 2.003(19), Pd–N(4) = 2.007(18), Pd–N(5) = 2.015(19), and Pd–N(8)$^{\#1}$ = 2.027(18) Å, symmetry code #1: $-x+1, y, -z+1/2$) of imidazolyl moiety from four separate ligands to furnish a square geometry, with the Pd···Pd distance of 6.810(3) Å. And the coordination angles of N–Pd–N range from 88.4(8)° to 92.4(8)° (Table 2). Further analysis reveals that the adjacent dinuclear cage units are further extended into 3D framework through the nonclassical weak π···π stacking interactions between the parallel phenyl rings (Fig. 2b) [23,24]. The

Table 1
The crystal parameters, data collection and refinement results for **4**–**6**.

	4	**5**	**6**
Chemical formula	$C_{60}H_{72}N_{20}O_{16}Pd_2S_2$	$C_{30}H_{32}Br_4N_8Pd_2$	$C_{44}H_{68}Cl_4N_8O_6Pd_2S_4$
Formula weight	1606.29	1037.07	1287.90
T (K)	100(2)	120(2)	100(2)
Crystal system	monoclinic	monoclinic	monoclinic
Space group	*C*2/*c*	*C*2/*m*	$P2_1/c$
a (Å)	26.3427(7)	16.790(3)	11.9806(5)
b (Å)	13.6628(3)	17.633(3)	18.9711(8)
c (Å)	20.3857(5)	9.0145(19)	12.0880(4)
α (°)	90	90	90
β (°)	111.450(3)	118.21(3)	94.580(3)
γ (°)	90	90	90
V (Å^3)	6828.9(3)	2351.9(9)	2738.65(19)
Z	4	2	2
D_{calc} (g cm^{-3})	1.562	1.464	1.562
μ (mm^{-1})	0.670	4.187	1.056
F (000)	3296	1000	1320
Reflections collected	16189	8310	24185
Unique reflections	6934	2418	5553
R_{int}	0.0211	0.0451	0.0482
R^a, wR^b ($I > 2\sigma(I)$)	0.0295, 0.0725	0.0830, 0.2560	0.0596, 0.1262
Goodness-of-fit (GOF) on F^2	0.952	1.047	1.133

[a] $R = \sum||F_o| - |F_c||/\sum|F_o|$.
[b] $wR = |\sum w(|F_o|^2 - |F_c|^2)|/\sum|w(F_o)^2|^{1/2}$, where $w = 1/[\sigma^2(F_o^2) + (aP)^2 + bP]$. $P = (F_o^2 + 2F_c^2)/3$.

Table 2
Selected bond lengths (Å) and angles (°) for compounds **4**–**6**.[a]

*Complex **4***					
Pd–N(1)$^{\#1}$	2.003(19)	Pd–N(4)	2.007(18)	Pd–N(5)	2.015(19)
Pd–N(8)$^{\#1}$	2.027(18)				
N(1)$^{\#1}$–Pd–N(4)	89.8(8)	N(1)$^{\#1}$–Pd–N(8)$^{\#1}$	88.4(8)	N(4)–Pd–N(5)	89.2(8)
N(5)–Pd–N(8)$^{\#1}$	92.4(8)				
*Complex **5***					
Pd–N(1)	1.990(11)	Pd–Br	2.431(4)	N(1)–Pd–Br	91.3(3)
N(1)$^{\#2}$–Pd–Br	88.6(3)	N(1)–Pd–N(1)$^{\#2}$	177.1(6)	Br–Pd–Br$^{\#2}$	178.6(3)
*Complex **6***					
Pd–N(1)	2.031(4)	Pd–N(4)$^{\#3}$	2.017(4)	Pd–Cl(2)	2.292(13)
Pd–Cl(1)	2.304(13)				
N(4)$^{\#3}$–Pd–N(1)	176.4(16)	Cl(2)–Pd–Cl(1)	175.1(5)	N(1)–Pd–Cl(2)	90.5(12)
N(1)–Pd–Cl(1)	91.2(12)	N(4)$^{\#3}$–Pd–Cl(2)	89.2(13)	N(4)$^{\#3}$–Pd–Cl(1)	89.4(12)

[a] Symmetry codes: #1 $-x+1, y, -z+1/2$; #2 $-x, y, -z$; #3 $-x-1, -y-1, -z$.

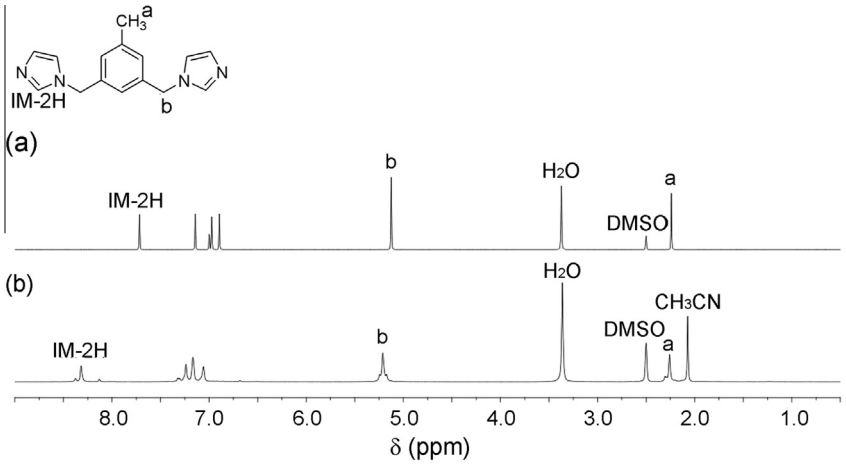

Fig. 1. ^{1}H NMR spectrum for **2** with $PdBr_2(CH_3CN)_2$ in DMSO-d_6 at 293 K: (a) the metal-free ligand **2**, and (b) **2**/$PdBr_2(CH_3CN)_2$ = 1:1.

centre-to-centre distance between the planes of two phenyls from different cages (Cg(1)···Cg(1)$^{\#1}$, Cg(1): C(5)–C(6)–C(7)–C(8)–C(9)–C(10) and symmetry code #1: $1-x, 1-y, 1-z$) with a dihedral angle of 0° is 4.066(15) Å, and the centroid–centroid distance and the dihedral angle between the other two phenyl rings (Cg(2)···Cg(2)$^{\#2}$, Cg(2): C(19)–C(20)–C(21)–C(22)–C(23)–C(24) and symmetry code #2: $1-x, 2-y, 1-z$) are 4.172(14) Å and 0°, respectively, stabilizing the resulting crystal structure (Table 3). More interestingly, the cage aggregates are stacked along the crystallographic *b* axis to create one-dimensional channels (Fig. 2c). It should be noted that two different type of crystallographic NO_3^- anions (A and B) are found in the asymmetric unit. In the middle of each adjacent channel, two NO_3^- (A) each lie about other independent inversion centres, between which weak C–H···O interactions (C(1)···O(5) = 3.207(2) Å, C(21)···O(6) = 3.157(3) Å, C(15)···O(7) = 3.124(3) Å and C(29)···O(8) = 3.297(6) Å, Table 4) are observed. By comparison, the other two NO_3^- (B) adopt an *anti*-configuration mode outside of every adjacent column. Each anion is H-bonded to the adjacent water (O(9)···O(3) = 2.890(4) Å, O(9)–H(9)···O(3) = 172(3)°), which further assembles with DMSO molecule through hydrogen bonding interaction with distance of 2.750(3) Å (O(9)···O(1)) to give an infinite offset 1D chain (Fig. 2c). In addition, there are also extra C–H···O interactions (C(17)···O(2) = 3.210(4) Å, C(3)···O(3) = 3.184(3) Å, and C(13)···O(9) = 3.165(4) Å, Table 4) among the anions, solvents and ligands to strengthen the overall structure of complex **4**. It is worth mentioning here that the anions involved in connecting the cage aggregates to 1D channel structures is not a common phenomenon. Furthermore, these results suggest that solvent molecules play an important role in crystallizing and stabilizing the conformation of the native crystals, owing to their ability to form hydrogen bonds with the host structure [25].

3.3. Structural description of $[Pd_2(\mathbf{2})_2Br_4]_n$ (**5**)

To further investigate the influence of counteranions on the formation of the supramolecular frameworks, palladium bromide is employed to react with the similar exo-bidentate ligand **2**. X-ray diffraction analyses show that the resulting complex **5** has a monoclinic space group *C*2/*m* and exhibits a twisted centrosymmetric [2+2] parallelogram structure composed of two Pd(II) ions doubly bridged to one another by means of two organic ligands, which is further held together by weak stacking and hydrogen bonding interactions to result in quite different 3D architectures from complex **4** (Fig. 3).

Owing to the binding affinity of Pd^{2+} to the anions (NO_3^- < Br^- ~ Cl^-) [26], in **5**, every palladium atom is coordinated with a slightly distorted square planar geometry by two terminal bromides anions and two nitrogen atoms belonging to imidazolyl units of two distinct ligands, which are orientated *trans* to one another. In each dinuclear metallocyclic unit, the Pd···Pd distance is 8.072(4) Å. The bond distances of Pd–N and Pd–Br are 1.990(11) Å and 2.431(4) Å, respectively; the N–Pd–N coordination angle is 177.1(6)° (Table 2). As depicted in Fig. 3b, infinite

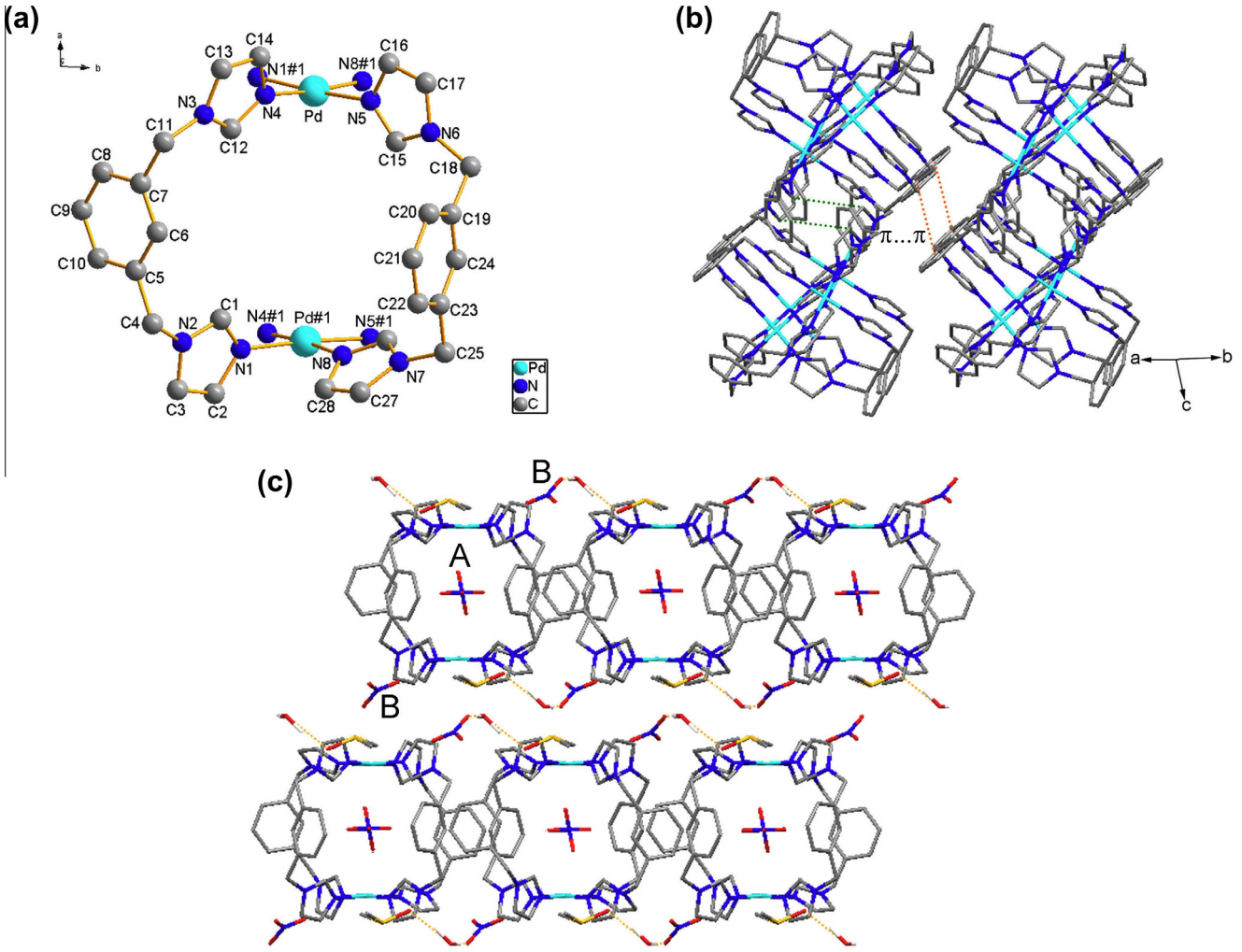

Fig. 2. (a) The asymmetric unit of distorted $[Pd_2(\mathbf{1})_2]$ dinuclear metallocyclic structure. Hydrogen atoms, anions and solvents were omitted for clarity. (b) The 3D framework of **4** formed by the weak π···π stacking interactions between the parallel phenyl rings. Green and orange dashed lines indicate π···π interactions in the same column and in the different columns, respectively. (c) A perspective view of the 1D channel structure with the infinite offset chain by the hydrogen bonding interactions between solvents and anions viewed along the *b* axis. The O–H···O interactions are emphasized in dashed lines. (For interpretation of the references to color in this figure legend, the reader is referred to the web version of this article.)

Table 3
Selected nonclassical weak π···π interactions for complex **4**.[a]

Cg(*I*)[b]	Cg(*J*)	Cg–Cg[c] (Å)	Dihedral angles (°)
Cg(1)	Cg(1)$^{\#1}$	4.066(15)	0
Cg(2)	Cg(2)$^{\#2}$	4.172(14)	0

[a] Symmetry codes: #1 1 − *x*,1 − *y*,1 − *z*; #2 1 − *x*,2 − *y*,1 − *z*.
[b] Cg(1): C(5)–C(6)–C(7)–C(8)–C(9)–C(10), Cg(2): C(19)–C(20)–C(21)–C(22)–C(23)–C(24), where Cg refers to the ring centre of gravity and the numbers represent the rings involved in the interactions.
[c] Cg–Cg: distance between ring centroids.

Table 4
H-bonding geometry (Å, °) for complex **4**.[a]

D–H···A	D–H	H···A	D···A	D–H···A (°)
O(9)–H(9)···O(1)$^{\#1}$	0.87	1.89	2.750(3)	168
O(9)–H(9)···O(3)	0.89	2.01	2.890(4)	172
C(1)–H(1)···O(5)	0.95	2.53	3.207(2)	129
C(3)–H(3)···O(3)$^{\#2}$	0.95	2.49	3.184(3)	130
C(13)–H(13)···O(9)	0.95	2.26	3.165(4)	160
C(15)–H(15)···O(7)	0.95	2.38	3.124(3)	135
C(17)–H(17)···O(2)$^{\#3}$	0.95	2.42	3.210(4)	141
C(21)–H(21)···O(6)$^{\#4}$	0.95	2.33	3.157(3)	145
C(29)–H(29)···O(8)$^{\#5}$	0.98	2.33	3.297(6)	168

[a] Symmetry codes: #1 1/2 − *x*,3/2 − *y*,1 − *z*; #2 1 − *x*,1 − *y*,1 − *z*; #3 *x*,1 + *y*,*z*; #4 1 − *x*,2 − *y*,1 − *z*; #5 −1/2 + *x*, −1/2 + *y*,*z*.

ladder-like chains in a criss-crossed fashion are observed along the crystallographic *b* axis. Notably, there exist weak π···π stacking interactions between the imidazole rings with a centre-to-centre distance of 4.190(11) Å and weak C–H···Br hydrogen bonds (C(4)···Br = 3.823(1) Å), which may play an important role in stabilizing the whole crystal structure of **5**. Viewed along the crystallographic *c* axis, the metallocyclic motifs of **5** pile up to form large 1D channels in the crystalline solid state (Fig. 3c). In the complex **5**, the exact number of non-coordianted solvent molecules in the crystallographic asymmetry unit could not be determined according to the Fourier electron densities due to disorder. However, the host framework could be located exactly. Considering strong disorganization of the included solvent molecules and the resulting low scattering power of the crystals of **5**, we corrected the observed data by using the SQUEEZE routine in PLATON [27]. When removing free solvent molecules, the vacant channels are approximately rectangular in cross-section with internal van der Waals dimensions of

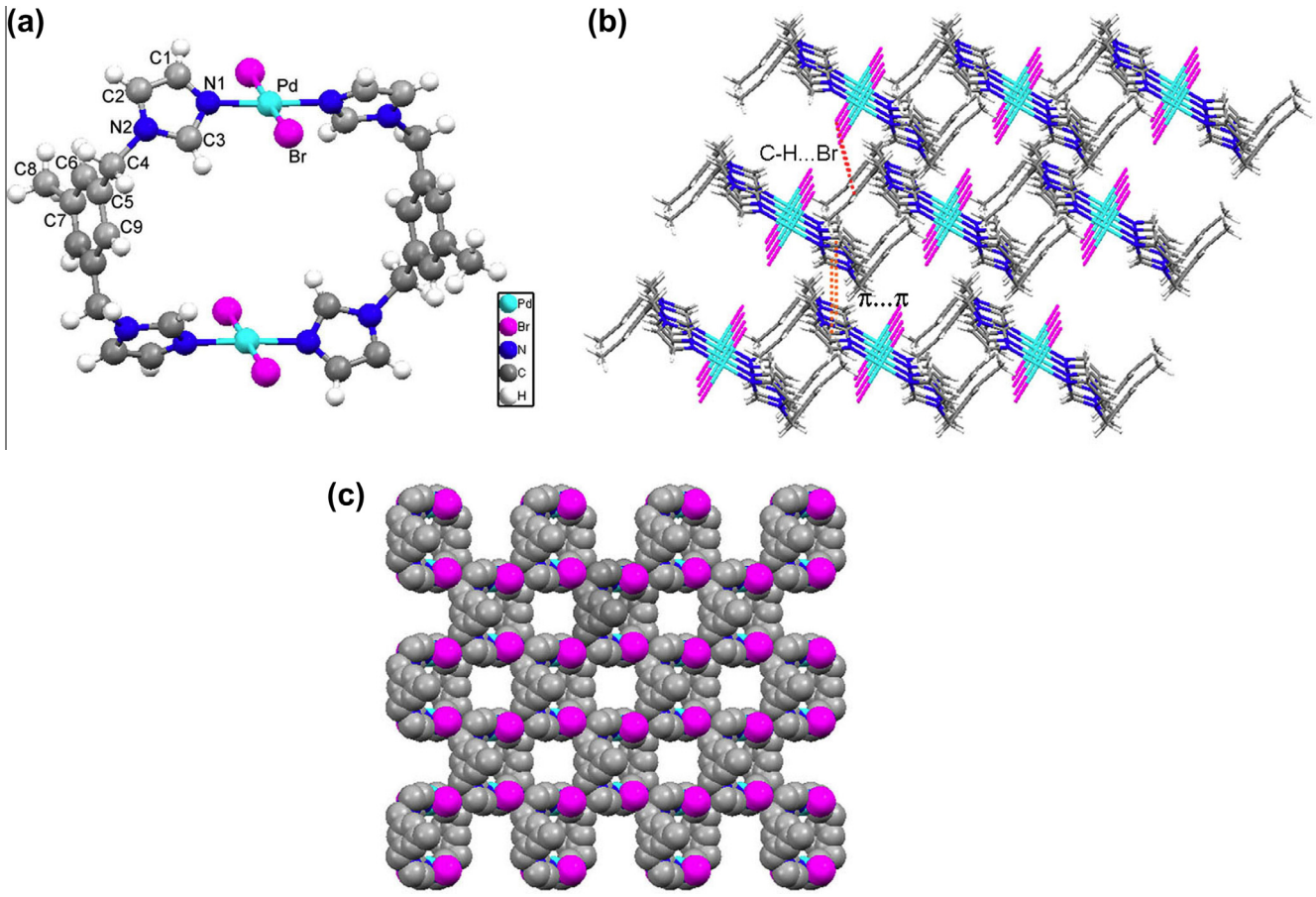

Fig. 3. (a) The asymmetric unit of $[Pd_2(\mathbf{2})_2Br_4]_n$ (**5**). (b) Packing of **5** viewed along the crystallographic *b* axis. Orange dashed lines indicate weak π···π interactions between the parallel imidazole rings and the weak C–H···Br interactions are emphasized in red dashed lines. (c) View of 1D channels of **5** along the crystallographic *c* axis. (For interpretation of the references to colour in this figure legend, the reader is referred to the web version of this article.)

ca. 4.8 × 7.0 Å^2, and the effective free volume of **5** calculated using PLATON is 32.5% [28]. Unlike complex **4** discussed above, no obvious secondary interactions such as H-bonding are observed between these dinuclear motifs and solvents in **5**. It is inferred that the assembled systems of Pd(II) ions and flexible imidazole-based ligands are sensitive to counteranions.

3.4. Structural description of $\{[Pd_2(\mathbf{3})_2Cl_4]\cdot 4DMSO\}_n$ (**6**)

Compared with complex **5**, in order to further understand the influence of the additional functional sites of chosen ligands on the construction of supramolecular frameworks, ligand **3** containing N, O donors with high steric hindrance is introduced, which leads to a new complex **6**. X-ray analysis reveals that crystal **6** is solved in monoclinic space group $P2_1/c$. The fundamental building unit of **6** contains a discrete rectangular complex with internal van der Waals dimensions of *ca.* 3.6 × 7.3 Å^2. The asymmetric unit of **6** is comprised of one 4-coordinated Pd(II) center, one ligand **3**, two terminal chlorides and two crystallographically independent DMSO molecules (Fig. 4a). That is, one DMSO solvent is coordinated with the hydroxyl group of ligand through O–H···O hydrogen bond (O(1)···O(2) = 2.611(6) Å, O(1)–H(1A)···O(2) = 166(9)°) and the other is relatively free in the loop (Table 5). In **6**, the Pd–N lengths and the Pd–Cl lengths are in the range of 2.017(4)–2.031(4) Å and 2.292(13)–2.304(13) Å, respectively, and the N–Pd–N angle is 176.4(16)° (Table 2). As shown in Fig. 4b, the ring-like units are connected by intermolecular π···π stacking interactions between two parallel adjacent imidazole rings (centroid–centroid distance = 3.473(3) Å and dihedral angle = 0°) to produce a 1D chain structure. These supramolecular chains are further stacked to generate a 2D undulating framework (Fig. 4c). Owing to the steric blocking of the substituent *t*-butyl of **3**, the metallocyclic units and the 2D layer are not in a plane, the phenyl rings of ligands can protrude into the cavities of the adjacent loops. Significantly, the two type of DMSO molecules in the lattice both adopt *anti*-configuration modes to lie on each side of the adjacent column. Moreover, the arrangement is further stabilized by weak C–H···O hydrogen bonds (C(3)···O(3) = 3.151(8) Å, C(11)···O(2) = 3.251(7) Å, C(14)···O(2) = 3.158(7) Å, C(20)···O(3) = 3.305(10) Å) (Table 5). In contrast to **5**, the DMSO solvents are involved in complexation to occupy the cavity of the dinuclear unit and confirm to facilely result in the formation of the wavelike 2D structure. Consequently, the distinct assemblies architectures with Pd(II) ions could be exclusively attributed to the presence of substituents (e.g. hydroxy and *t*-butyl groups) in the phenyl ring.

3.5. X-ray powder diffraction

In order to characterize the structural homogeneity of these complexes, powder XRD (PXRD) patterns of complexes **4**–**6** were performed. Although minor differences can be observed in the positions, intensities and widths of some peaks, the experimental pattern favorably correlates with the simulated one generated from the single crystal X-ray diffraction data (Fig. 5). The matching of the PXRD's suggests that the bulk powder has a single phase with a similar structure to the single crystal.

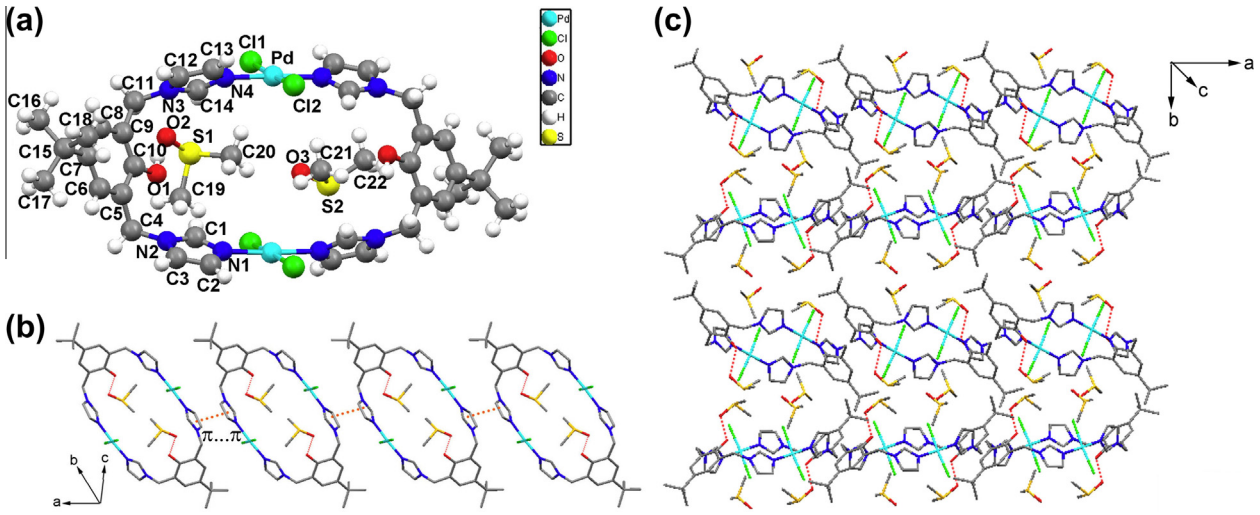

Fig. 4. (a) The asymmetric unit of $\{[Pd_2(\mathbf{3})_2Cl_4]\cdot 4DMSO\}_n$ (**6**). (b) A 1D chain of complex **6** formed by the intermolecular π···π stacking interactions (orange dashed lines) between the parallel imidazole rings. The red dashed lines indicate the O–H···O hydrogen bonds between the hydroxyl groups and the coordinated solvents. (c) Views of the wavelike 2D framework of **6**. (For interpretation of the references to color in this figure legend, the reader is referred to the web version of this article.)

Table 5
Selected H-bonding geometry (Å, °) for $\{[Pd_2(\mathbf{3})_2Cl_4]\cdot 4DMSO\}_n$ (**6**).[a]

D–H···A	D–H	H···A	D···A	D–H···A (°)
O(1)–H(1)···O(2)$^{\#1}$	0.85	1.78	2.611(6)	166
C(3)–H(3)···O(3)$^{\#2}$	0.95	2.22	3.151(8)	165
C(11)–H(11)···O(2)$^{\#1}$	0.99	2.40	3.251(7)	143
C(14)–H(14)···O(2)$^{\#1}$	0.95	2.39	3.158(7)	138
C(20)–H(20)···O(3)	0.98	2.44	3.305(10)	147

[a] Symmetry codes: #1 $-x,-1/2+y,1/2-z$; #2 $-1+x,y,z$.

3.6. Thermogravimetric analysis

To estimate the thermal stabilities of complexes **4**–**6**, thermogravimetric analysis (TGA) experiments are carried out from 30 to 750 °C. TGA curves for complexes **4**–**6** are shown in Fig. 6. For complex **4**, a gradual weight loss (observed, 2.30%; calculated, 2.24%) from room temperature to 140 °C is consistent with the loss of water molecules, and from 285 °C the composition of the host framework begins to collapse. For complex **5**, the weight loss corresponding to the release of the lattice DMSO molecules occur from 100 to 182 °C. The observed weight loss of 13.05% is in agreement with the calculated 13.07%. At above 325 °C, the framework begins to decompose slowly. In complex **6**, 24.15% weight loss shows that the coordinated DMSO molecules (calculated, 24.22%) are lost from 160 to 195 °C, and the decomposition temperature of the residual composition spans the range of 300–550 °C.

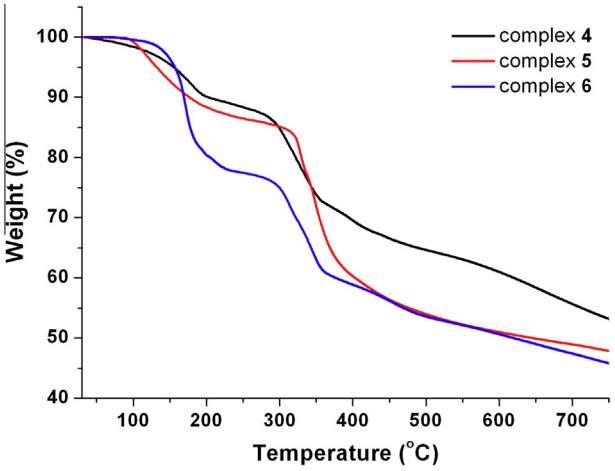

Fig. 6. The TG plots of complexes **4**–**6**.

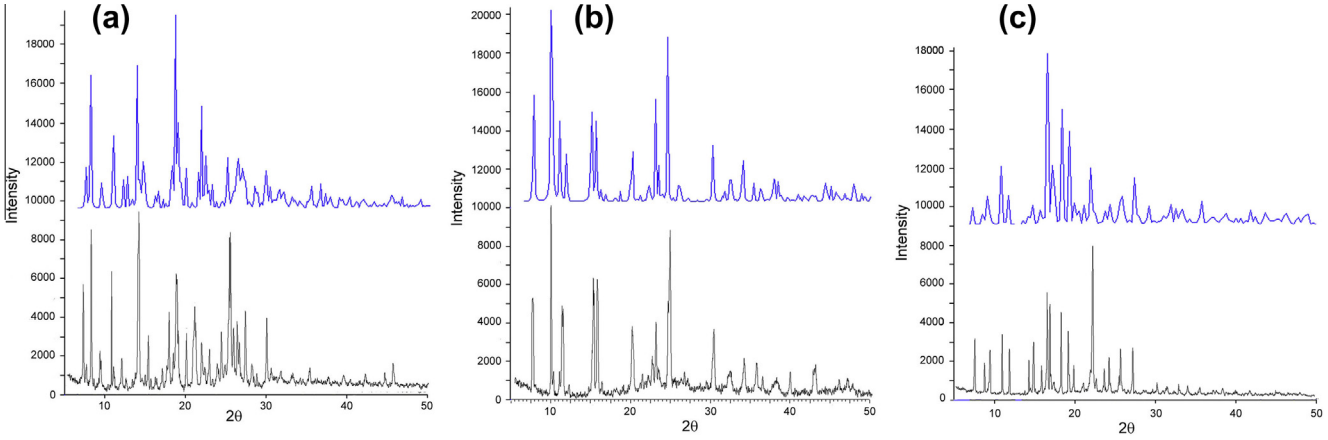

Fig. 5. Comparison of powder X-ray diffraction patterns of (a) complex **4**; (b) complex **5**; (c) complex **6**: the top and bottom patterns correspond to the simulated and experimental results, respectively.

4. Conclusion

In conclusion, three new interesting supramolecular complexes have been successfully assembled by utilizing the flexible exo-bidentate imidazole-containing ligands and divalent palladium salts. Although all complexes have the similar dinuclear metallocyclic building blocks, crystal **4** exhibits a [4+2] lantern-like cage structure, complex **5** shows a 1D channel and **6** presents a 2D undulating framework. These results demonstrate that the nature and coordination motifs of the final supramolecular architectures strongly rely on the additional functional sites of chosen ligands. In addition, the steric hindrance caused by the presence of substituents in the aryl ring of the ligands could also influence the structures of aggregates. Moreover, our study shows that the noncovalent interactions such as intermolecular $\pi\cdots\pi$ stacking interactions (especially between imidazolyl groups) and hydrogen bonds (e.g., O–H$\cdots$O, C–H$\cdots$O, C–H$\cdots$Br) may play important roles in the aspect of linking low-dimensional entities into high-dimensional supramolecular networks. This work does not only deepen our systemic understanding of the structural functionality of the flexibility of the imidazole ligands but also provide new perspectives for generating new discrete macrocyclic and cage-like metal–organic frameworks to enrich the field of crystal engineering. Investigations of using the strategy depending on coordination complexes as building blocks to construct functional supramolecular assemblies for possible practical use are in progress.

Acknowledgments

This work was supported by the National Natural Science Foundation of China (No. 21202134), and the Research Fund for the Doctoral Program of Southwest University of Science and Technology (No. 10zx7120). We thank the Centre of Testing & Analysis, Sichuan University for PXRD, and NMR measurements.

Appendix A. Supplementary data

CCDC 878309 (**4**), CCDC-759096 (**5**) and CCDC-759097 (**6**) contains the supplementary crystallographic data for this paper. These data can be obtained free of charge from The Cambridge Crystallographic Data Centre via http://www.ccdc.cam.ac.uk/data_request/cif. Supplementary data associated with this article can be found, in the online version, at http://dx.doi.org/10.1016/j.ica.2013.07.014.

References

[1] (a) S. Leininger, B. Olenyuk, P.J. Stang, Chem. Rev. 100 (2000) 853;
(b) W.L. Leong, J.J. Vittal, Chem. Rev. 111 (2011) 688.
[2] (a) Y.-B. Zhang, W.-X. Zhang, F.-Y. Feng, J.-P. Zhang, X.-M. Chen, Angew. Chem., Int. Ed. 48 (2009) 5287;
(b) K. Sumida, M.R. Hill, S. Horike, A. Dailly, J.R. Long, J. Am. Chem. Soc. 131 (2009) 15120;
(c) S. Bourrelly, B. Moulin, A. Rivera, G. Maurin, S. Devautour-Vinot, C. Serre, T. Devic, P. Horcajada, A. Vimont, G. Clet, M. Daturi, J.-C. Lavalley, S. Loera-Serna, R. Denoyel, P.L. Llewellyn, G.J. Férey, J. Am. Chem. Soc. 132 (2010) 9488.
[3] (a) J. Pang, E.J.-P. Marcotte, C. Seward, R.S. Brown, S. Wang, Angew. Chem., Int. Ed. 40 (2001) 4042;
(b) M.D. Allendorf, C.A. Bauer, R.K. Bhakta, R.J.T. Houk, Chem. Soc. Rev. 38 (2009) 1330.
[4] (a) A.A. Belik, K. Kodama, N. Igawa, S. Shamoto, K. Kosuda, E. Takayama-Muromachi, J. Am. Chem. Soc. 132 (2010) 8137;
(b) J.S. Miller, D. Gatteschi, Chem. Soc. Rev. 40 (2011) 3065.
[5] Y. Liu, G. Li, X. Li, Y. Cui, Angew. Chem., Int. Ed. 46 (2007) 6301.
[6] M. Yoon, R. Srirambalaji, K. Kim, Chem. Rev. 112 (2012) 1196.
[7] M. Plabst, L.B. McCusker, T. Bein, J. Am. Chem. Soc. 131 (2009) 18112.
[8] (a) C.-P. Li, M. Du, Chem. Commun. 47 (2011) 5958;
(b) H. Deng, C.J. Doonan, H. Furukawa, R.B. Ferreira, J. Towne, C.B. Knobler, B. Wang, O.M. Yaghi, Science 327 (2010) 846;
(c) J.J. Zhang, L. Wojtas, R.W. Larsen, M. Eddaoudi, M.J. Zaworotko, J. Am. Chem. Soc. 131 (2009) 17040.
[9] D. Zhao, D.J. Timmons, D. Yuan, H.-C. Zhou, Acc. Chem. Res. 44 (2010) 123.
[10] (a) Y. Wan, L. Zhang, L. Jin, S. Gao, S. Lu, Inorg. Chem. 42 (2003) 4985;
(b) M. Eddaoudi, J. Kim, J.B. Wachter, H.K. Chae, M. O'Keeffe, O.M. Yaghi, J. Am. Chem. Soc. 123 (2001) 4368.
[11] (a) P.J. Steel, Acc. Chem. Res. 38 (2005) 243;
(b) G.-X. Liu, Y.-Q. Huang, Q. Chu, T. Okamura, W.-Y. Sun, H. Liang, N. Ueyama, Cryst. Growth Des. 8 (2008) 3233;
(c) M.-L. Zhang, D.-S. Li, J.-J. Wang, F. Fu, M. Du, K. Zou, X.-M. Gao, Dalton Trans. (2009) 5355.
[12] N.C. Gianneschi, M.S. Masar, C.A. Mirkin, Acc. Chem. Res. 38 (2005) 825.
[13] C.G. Oliveri, P.A. Ulmann, M.J. Wiester, C.A. Mirkin, Acc. Chem. Res. 41 (2008) 1618.
[14] R. Chakrabarty, P.S. Mukherjee, P.J. Stang, Chem. Rev. 111 (2011) 6810.
[15] J.B. Pollock, T.R. Cook, P.J. Stang, J. Am. Chem. Soc. 134 (2012) 10607.
[16] Selected examples, see (a) H.Y. Bai, J.F. Ma, J. Yang, L.P. Zhang, J.C. Ma, Y.Y. Liu, Cryst. Growth Des. 10 (2010) 1946;
(b) L.L. Li, R.X. Yuan, L.L. Liu, Z.G. Ren, A.X. Zheng, H.J. Cheng, H.X. Li, J.P. Lang, Cryst. Growth Des. 10 (2010) 1929;
(c) J.-G. Wang, N. Chai, S.-C. Wang, L.-F. Ma, L.-Y. Wang, Inorg. Chem. Commun. 30 (2013) 143;
(d) L. Dobrzańska, G.O. Lloyd, H.G. Raubenheimer, L.J. Barbour, J. Am. Chem. Soc. 128 (2006) 698;
(e) J. Yang, J.-F. Ma, Y.-Y. Liu, J.-C. Ma, S.R. Batten, Cryst. Growth Des. 8 (2008) 4383;
(f) L. Carlucci, G. Ciani, S. Maggini, D.M. Proserpio, Cryst. Growth Des. 8 (2008) 162.
[17] P.S. Mukherjee, N. Das, Y.K. Kryschenko, A.M. Arif, P.J. Stang, J. Am. Chem. Soc. 126 (2004) 2464. and references therein.
[18] S. Zhang, Y. Tang, Y. Su, J. Lan, R. Xie, J. You, Inorg. Chim. Acta 362 (2009) 1511.
[19] S. Zhang, J. Lan, Z. Mao, R. Xie, J. You, Cryst. Growth Des. 8 (2008) 3134.
[20] S. Zhang, S. Yang, J. Lan, Y. Tang, Y. Xue, J. You, J. Am. Chem. Soc. 131 (2009) 1689.
[21] L. Yang, L. Luo, S. Zhang, X. Su, J. Lan, C.-T. Chen, J. You, Chem. Commun. 46 (2010) 3938.
[22] G.M. Scheldrick, SHELX-97 and SHELXL-97, Program for Solution and Refinement of Crystal Structures, University of Göttingen, Germany, 1997.
[23] C. Janiak, J. Chem. Soc., Dalton Trans. (2000) 3885.
[24] C. Ren, L. Hou, B. Liu, G.-P. Yang, Y.-Y. Wang, Q.-Z. Shi, Dalton Trans. 40 (2011) 793.
[25] (a) S. Pal, N.B. Sankaran, A. Samanta, Angew. Chem., Int. Ed. 42 (2003) 1741;
(b) S.L. Li, Y.Q. Lan, J.C. Ma, J.F. Ma, Z.M. Su, Cryst. Growth Des. 10 (2010) 1161.
[26] (a) C.-Y. Chen, P.-Y. Cheng, H.-H. Wu, H.M. Lee, Inorg. Chem. 46 (2007) 5691;
(b) H. Maeda, Chem. Eur. J. 14 (2008) 11274.
[27] (a) A.L. Spek, Acta Crystallogr., Sect. D 65 (2009) 148;
(b) M. Mastalerz, M.W. Schneider, I.M. Oppel, O. Presly, Angew. Chem., Int. Ed. 50 (2011) 1046;
(c) M. Xue, C.-F. Chen, Chem. Commun. 47 (2011) 2318;
(d) L. Yang, F. Yang, J. Lan, G. Gao, J. You, X. Su, Org. Biomol. Chem. 9 (2011) 2618.
[28] (a) A.L. Spek, PLATON, A Multipurpose Crystallographic Tool, Utrecht University, Utrecht, The Netherlands, 2001;
(b) A.L. Spek, J. Appl. Crystallogr. 36 (2003) 7.